

# Self-organization of pulsing and bursting in a CO<sub>2</sub> laser with opto-electronic feedback

Joana G. Freire,<sup>1,2,3</sup> Riccardo Meucci,<sup>1,2,4</sup> Fortunato Tito Arcelli,<sup>4,5</sup>  
 and Jason A. C. Gallas<sup>1,2,3,4,6,7</sup>

<sup>1</sup>Departamento de Física, Universidade Federal da Paraíba, 58051-970 João Pessoa, Brazil

<sup>2</sup>Instituto de Altos Estudos da Paraíba, Rua Infante Dom Henrique 100-1801, 58039-150 João Pessoa, Brazil

<sup>3</sup>CELC, Departamento de Matemática, Universidade de Lisboa, 1649-003 Lisboa, Portugal

<sup>4</sup>Istituto Nazionale di Ottica, Consiglio Nazionale delle Ricerche, Largo E. Fermi 6, Firenze, Italy

<sup>5</sup>Università di Firenze, 50019 Sesto Fiorentino, Firenze, Italy

<sup>6</sup>Institute for Multiscale Simulations, Friedrich-Alexander Universität, D-91052 Erlangen, Germany

<sup>7</sup>Max-Planck Institute for the Physics of Complex Systems, Nöthnitzer Str. 38, 01187 Dresden, Germany

(Received 12 January 2015; accepted 16 March 2015; published online 8 April 2015)

We report a detailed investigation of the stability of a CO<sub>2</sub> laser with feedback as described by a six-dimensional rate-equations model which provides satisfactory agreement between numerical and experimental results. We focus on experimentally accessible parameters, like bias voltage, feedback gain, and the bandwidth of the feedback loop. The impact of decay rates and parameters controlling cavity losses are also investigated as well as control planes which imply changes of the laser physical medium. For several parameter combinations, we report stability diagrams detailing how laser spiking and bursting is organized over extended intervals. Laser pulsations are shown to emerge organized in several hitherto unseen regular and irregular phases and to exhibit a much richer and complex range of behaviors than described thus far. A significant observation is that qualitatively similar organization of laser spiking and bursting can be obtained by tuning rather distinct control parameters, suggesting the existence of unexpected symmetries in the laser control space. © 2015 AIP Publishing LLC. [<http://dx.doi.org/10.1063/1.4916923>]

CO<sub>2</sub> laser with feedback is a complex system that has been investigated extensively both experimentally and through numerical simulations. As a result, a highly tested model exists for this laser, famed for providing quite satisfactory agreement between numerical and experimental observations. However, the laser involves a large number of freely tunable control parameters, whose impact on the laser performance and stability has not yet been investigated. In the present paper, we bridge this gap by performing a systematic numerical classification of complex dynamical phenomena observed in the CO<sub>2</sub> laser with feedback as a function of its several control parameters. More specifically, we report high-resolution stability diagrams for accessible control parameters and for parameters that imply more subtle changes of the physical characteristics of the laser medium. Such diagrams describe the self-organization and the extension of stable spiking and bursting laser phases. Laser pulsations are shown to display novel regular and irregular features. In particular, our stability diagrams suggest that the laser control space harbors remarkable symmetries that were not yet accounted for but which are experimentally accessible. In addition, our stability diagrams provide stringent tests of the reliability and accuracy of the laser model investigated, currently the best model available for such laser.

interest is to learn how to optimize the use of this powerful laser in applications and how to extract new theoretical insight from the knowledge of its dynamical characteristics. The reasons for the interest in this type of lasers come from many applications such as, e.g., coupling several lasers together to bypass the power limitations of individual lasers. Coupling lasers involves a plethora of new and unanticipated phenomena, such as, for example, the abundant emergence of random spiking and bursting, the synchronization of strongly pulsating lasers, and several other phenomena.<sup>4-7</sup>

About thirty years ago, CO<sub>2</sub> lasers were used in pioneering experiments to verify phenomena and scenarios predicted in the emergent field of nonlinear dynamics. The reason was due to the CO<sub>2</sub> laser versatility and relative handiness of its custom realization in well-equipped laboratories. In this framework, the observation of deterministic chaos in CO<sub>2</sub> lasers with cavity modulation near the relaxation frequency was of primary importance.<sup>8-13</sup> From this experiment, other observations followed, confirming that chaos is also present in an autonomous configuration such as the CO<sub>2</sub> laser with optoelectronic feedback.<sup>14</sup> Nowadays, applications involving optoelectronic and optical feedbacks in semiconductor lasers are widespread, specially in the field of secure communications which rests on the phenomenon of chaotic synchronization between a master and a slave laser.<sup>5,6</sup>

To better understand the aforementioned phenomena in coupled lasers, one first needs a thorough understanding of a single CO<sub>2</sub> laser. The solitary laser involves a large number of freely tunable control parameters whose impact on its stability

## I. INTRODUCTION

The dynamics of the CO<sub>2</sub> laser<sup>1,2</sup> has been the subject of several investigations in recent years.<sup>3-5</sup> Of particular

and performance, despite the large literature available, has not yet been investigated. Here, our aim is to bridge this gap through a systematic numerical classification of complex dynamical phenomena observed in the CO<sub>2</sub> laser with feedback as a function of its control parameters. More specifically, we present detailed stability diagrams for two situations, namely, for easily accessible control parameters, and for parameters not so easily accessible, that imply more subtle changes of the physical characteristics of the laser medium.

In Sec. II, we present the most significant steps in developing the laser model used here. Then, we introduce the model (Sec. III) and explain how to obtain high-resolution stability diagrams for the model (Sec. IV). Sec. V reports stability diagrams for several control parameter planes and describes their features. Finally, Sec. VI summarizes our conclusions and some open problems. In resonance with this focus issue of Chaos, our paper reviews what has already been done concerning CO<sub>2</sub> lasers with opto-electronic feedback, a very fruitful laser system, pointing out several attractive perspectives for future research.

## II. GENESIS OF THE MODEL

The simplest approach to model the dynamics of a single-mode homogeneously broadened CO<sub>2</sub> laser is by using two rate equations, one for the laser intensity and one for the population inversion between the two resonant levels. This description is appropriate for a class B laser, in the classification introduced by Arecchi *et al.*<sup>15</sup> The two-level model was used to interpret the chaotic dynamics emerging in this kind of laser when an electro-optic feedback is introduced. When complemented by a third equation describing the opto-electronic feedback, the two-level laser equations provide the basic three-dimensional model necessary to foresee local bifurcations leading to chaos after the destabilization of a limit cycle<sup>14</sup> and global bifurcations related to the presence of a homoclinic connection in the phase-space.<sup>16</sup> This work suggests how to observe competing instabilities by operating a CO<sub>2</sub> laser with feedback in a parameter range with coexisting equilibrium points. From local chaos originated around a stationary solution with nonzero laser output intensity (named solution “1”), it is possible to observe a transition to homoclinic chaos of the Shilnikov type around an apparent saddle focus (named solution “2”). In this regime, the trajectories also visit the unstable solution with zero laser output intensity (named solution “0”). For further details, see Figs. 2 and 3 of Ref. 16. Subsequent investigations revealed that it is not possible to find a stationary solution associated with this apparent saddle focus. This subtle and intriguing aspect in the global dynamics led to the investigation in more detail of the Q-switching dynamics of the CO<sub>2</sub> laser related to the build-up process of the laser intensity originating from a spontaneous emission process when the laser is below threshold. Such analysis revealed that the two-level model is not adequate to fit experimental observations. To overcome this difficulty, a four-level model was introduced. Such model accounts for non-radiative couplings of the two resonant levels of the vibrational bands to which they belong. A precise description of the passive Q-switching in a CO<sub>2</sub> laser

with intracavity saturable absorbers was given in Refs. 17–19. Such a configuration also led to the observation of homoclinic chaos.<sup>20–25</sup> The CO<sub>2</sub> laser with saturable absorber is equivalent to the CO<sub>2</sub> laser with feedback in the sense that homoclinic chaos is observed in both of them.

Later, the transient behavior in CO<sub>2</sub> lasers with slowly swept parameters around the laser threshold was explained by the four-level model with equal relaxation rates for the two vibrational bands.<sup>26</sup> In this experiment, the features of the relaxation oscillations affecting the laser intensity after the crossing of the laser threshold have been characterized depending on the sweep rate of the cavity losses. Exploring laser dynamics near the laser threshold, another feature appears when the pump parameter is slowly swept, that is, the presence of a delayed bifurcation. Such a phenomenon, theoretically foreseen by Mandel and Erneux,<sup>27</sup> was experimentally observed and correctly explained by the four-level model for the CO<sub>2</sub> laser.<sup>28</sup>

The analysis of the dynamical behavior of a Q-switched CO<sub>2</sub> laser revealed that the laser intensity in the nonlinear amplification regime and the long time relaxation process to the steady state are correctly explained only by using the four-level model with different relaxation rates of the two vibrational bands.<sup>29</sup> On the other hand, in the linear amplification regime, both models produce the same result. In the case of chaotic dynamics obtained by means of sinusoidal modulation of cavity losses or by opto-electronic feedback, the same considerations are still valid reinforcing the adequacy of the four-level model. The four-level model for the CO<sub>2</sub> laser consists of five differential equations involving the laser intensity  $I$ , the population of the lasing levels  $N_1$  and  $N_2$ , and the global population of the rotational manifolds  $M_1$  and  $M_2$ . Consequently, the dynamics of a CO<sub>2</sub> laser with electro-optic feedback is ruled by a set of six differential equations (six dimensional model). From a theoretical point of view, the validity of the four-level model was demonstrated by a global application of center manifold theory allowing the reduction of the number of variables from six to four.<sup>30</sup>

Successive experimental confirmations of the adequacy of the six dimensional model are reported in Ref. 31, where evidence of stabilization of periodic solutions embedded in the chaotic attractor of this system is provided. The adopted strategy to control chaos is based on the introduction of an additional feedback loop where a selective filtering of the subharmonic components of the chaotic laser intensity signal is performed. The final result of this filtering process is the rejection of the undesired subharmonic components responsible for chaos and the enhancement of the fundamental frequency component associated with the limit cycle stabilized in the phase space. The stabilization of homoclinic chaos to the fixed point solution in the phase space was demonstrated by the use of a derivative filter on the laser output intensity.<sup>32</sup> Also, in such a case, the six dimensional model is particularly suited for describing the controlled trajectory to the only existing fixed point solution with nonzero intensity.

Another class of experiments, exploring the role of chaotic synchronization induced by a sinusoidal forcing or by noise added in the feedback loop, drew attention to the high

susceptibility of the system in the vicinity of the saddle focus.<sup>33</sup> Since a small perturbation, including noise, is able to modify the global dynamics from chaos to periodicity and vice-versa, synchronization can be easily obtained in a chain of CO<sub>2</sub> lasers in the homoclinic regime with nearest neighbor coupling.<sup>34,35</sup>

### III. SIX-DIMENSIONAL MODEL

The six-dimensional model of a CO<sub>2</sub> laser with feedback is defined by the following nonlinear ordinary differential equations:<sup>36,47</sup>

$$\dot{x}_1 = k_0 x_1 (x_2 - 1 - k_1 \sin^2(x_6)), \quad (1)$$

$$\dot{x}_2 = -\Gamma_1 x_2 - 2k_0 x_1 x_2 + \gamma x_3 + x_4 + P_0, \quad (2)$$

$$\dot{x}_3 = -\Gamma_1 x_3 + x_5 + \gamma x_2 + P_0, \quad (3)$$

$$\dot{x}_4 = -\Gamma_2 x_4 + \gamma x_5 + z x_2 + z P_0, \quad (4)$$

$$\dot{x}_5 = -\Gamma_2 x_5 + z x_3 + \gamma x_4 + z P_0, \quad (5)$$

$$\dot{x}_6 = \beta(B_0 - x_6 - R x_1 / (1 + \alpha x_1)). \quad (6)$$

In these equations,  $x_1$  represents the laser output intensity,  $x_2$  the population inversion between the two resonant levels, while  $x_6$  stands for the feedback voltage signal which controls the cavity losses. These three coupled variables are sufficient to generate chaos. However, as discussed above, due to the interplay of the different energy levels of the CO<sub>2</sub> molecule, one must introduce three additional variables acting as linear filters, thereby increasing the overall dimension of the phase space from three to six.

The variables  $x_3$ ,  $x_4$ , and  $x_5$  account for exchanges between the two molecular levels resonant with the radiation field and the other rotational levels of the same vibrational band of the molecule. The parameter  $k_0$  controls the unperturbed cavity loss,  $k_1$  determines the modulation strength,  $\gamma$  is the coupling constant,  $\Gamma_1$  and  $\Gamma_2$  are population relaxation rates,  $P_0$  the pump parameter,  $z$  represents the effective number of rotational levels, and  $\beta, B_0, R, \alpha$  are, respectively, the bandwidth, the bias voltage, the amplification, and the saturation factors of the feedback loop. Following Pisarchik *et al.*,<sup>36</sup> as reference parameters for our calculations, we fix  $\Gamma_1 = 10.0643$ ,  $\Gamma_2 = 1.0643$ ,  $\alpha = 32.8767$ ,  $\beta = 0.4286$ ,  $k_0 = 28.5714$ ,  $k_1 = 4.5556$ ,  $z = 10$ ,  $\gamma = 0.05$ ,  $R = 160$ ,  $B_0 = 0.1026$ , and  $P_0 = 0.016$ .

### IV. COMPUTATIONAL DETAILS

Our results are displayed in two complementary types of stability diagrams: (i) the standard stability diagram based on Lyapunov exponents,<sup>37,38</sup> and (ii) the novel isospike diagrams,<sup>39–46</sup> a more fruitful type of stability diagrams based on counting the number of spikes contained in one period of the periodic oscillations.

To produce the stability diagrams, a parameter window of interest is covered with a mesh of  $N \times N$  equidistant points. For each point, the temporal evolution is obtained by

integrating numerically Eqs. (1)–(6) using the standard fourth-order Runge-Kutta algorithm with fixed time-step  $h = 0.01$ .

In the diagrams presented in Fig. 1, integrations were performed by scanning parameters horizontally from left to right, starting from an arbitrarily chosen initial condition,

$$(x_1, x_2, x_3, x_4, x_5, x_6) = (0.0011, 1.01, 1.05, 10.05, 10.3, 0),$$

proceeding to the right by “following the attractor,” namely, by using the values of  $x_1, x_2, x_3, x_4, x_5, x_6$  obtained at the end of a calculation for a given parameter to start a new calculation after incrementing the parameter horizontally. In other words, instead of re-initializing initial conditions after changing the parameter, we simply kept the conditions that were already stored in the computer buffer due to the previous computation. This procedure was repeated for every parameter in the vertical axis. Similarly, in Figs. 2, 3, and 6, parameters were scanned horizontally but from right to left. In Figs. 4, 7, and 8, the initial condition above was used for all points on the mesh. These initializations guarantee that the integrations were not trapped by unimportant fixed points. In all cases, the first  $2 \times 10^5$  integration steps were discarded as a transient time needed to approach the attractor. The subsequent  $40 \times 10^5$  steps were used to compute the six exponents forming the Lyapunov spectrum.

To obtain isospike diagrams, namely, to find the number of spikes in a period of the oscillations, subsequent to the computation of the Lyapunov exponents, we continued integrations for an additional  $40 \times 10^5$  time-steps recording up to 800 extrema (maxima and minima) of the variable of interest and checking whether pulses repeated or not. In the isospike diagrams, we use a palette of 17 colors to represent the number of spikes contained in one period of the oscillations, as indicated by the colorbars in the Figures. Patterns with more than 17 spikes are plotted by recycling the 17 basic colors modulo 17. Black represents “chaos” (i.e., lack of numerically detectable periodicity), white and orange colors mark non-oscillatory solutions, if any, having, respectively, non-zero or zero amplitudes of the variable under consideration. Isospike diagrams can be also efficiently implemented to deal with experimental data.<sup>43</sup>

### V. STABILITY DIAGRAMS

We start by comparing both types of stability diagrams described in Sec. IV. They are plotted for the parameters considered most frequently in the literature, namely, as a function of the feedback gain  $R$  and the bias voltage  $B_0$ . The leftmost panel of Fig. 1 shows a standard Lyapunov stability diagram for the laser. In this diagram, gray shadings represent periodic oscillations (i.e., negative exponents) while the colors denote chaos (positive exponents). A similar Lyapunov stability diagram showing a smaller stability region and slightly distinct parameter values was given in Fig. 5(c) of Ref. 47. In contrast, the rightmost panel shows the isospike diagram corresponding to the Lyapunov diagram.

Comparing both diagrams on the top row of Fig. 1, it becomes obvious that the isospike diagram contains much

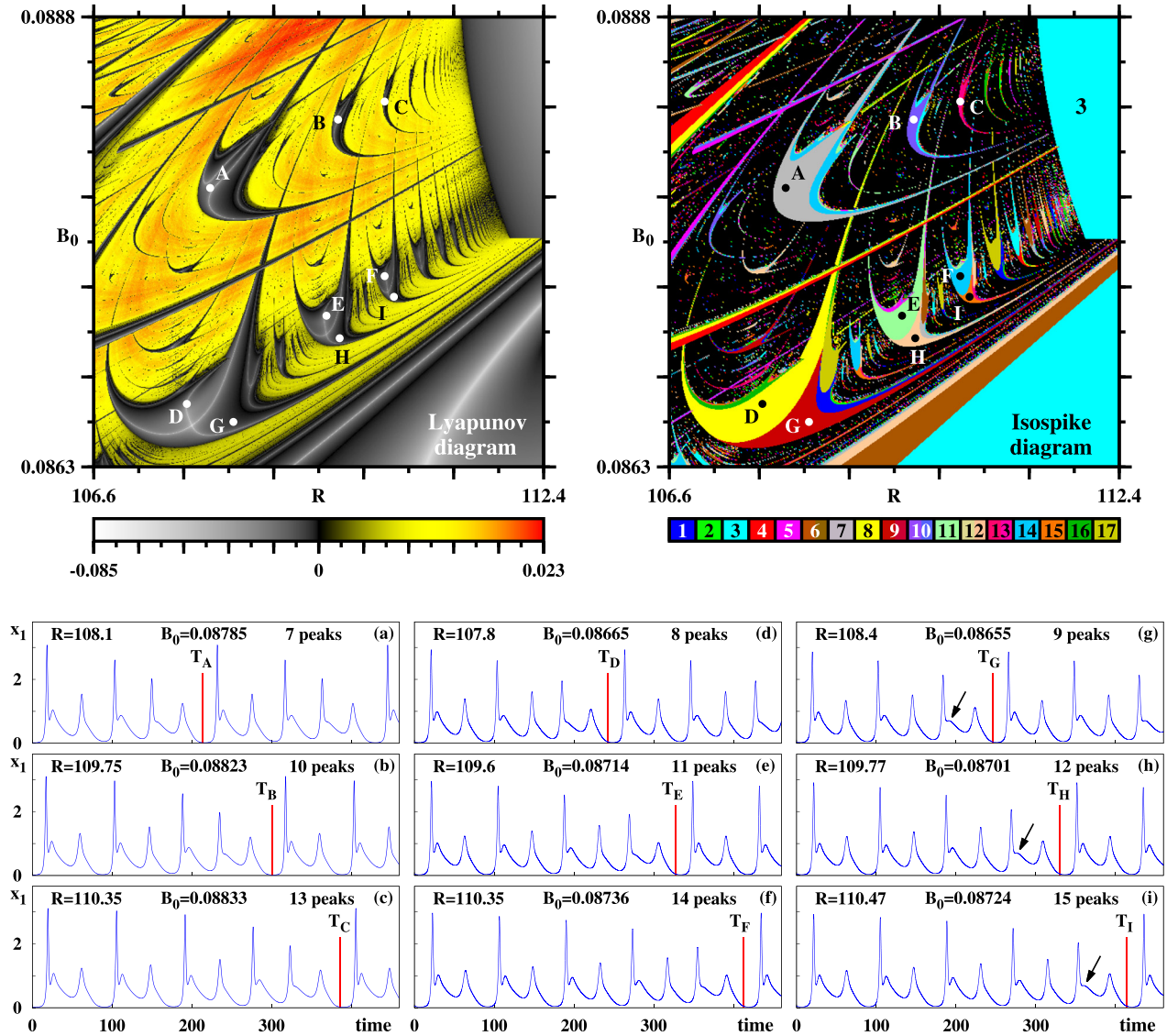


FIG. 1. Two alternative representations of the laser stability as a function of the feedback gain  $R$  and bias voltage  $B_0$ . Top left: standard Lyapunov stability diagram,<sup>13</sup> where gray shadings mark periodic oscillations (negative exponents), and colors denote chaos (positive exponents). Top right: Isospike diagram (see text), where colors display the number of spikes in one period of the laser intensity  $x_1$  and black denotes chaos (i.e., lack of numerically detectable periodicity). The isospike diagram contains by far much more information than the Lyapunov diagram. The number 3 marks the domain towards which both 3-spikes adding cascades accumulate. Panels (a)–(i) show temporal evolutions of intensity pulses for selected parameters, indicated by labeled dots in both diagrams. The oscillation periods  $T_\ell$  are given in the text. Black arrows in panels (g)–(i) indicate where new peaks are born (see text). For convenience, the vertical axis shows  $10^3 x_1$ .

more information than the Lyapunov diagram. Both diagrams clearly discriminate regular from chaotic oscillations. However, the isospike diagram informs simultaneously how the complexification of the laser signal occurs, i.e., it shows how to tune parameters in order to obtain more and more spikes in the laser oscillation via continuous deformations that create and destroy peaks, as described recently for the infinite-dimensional Mackey-Glass delayed feedback system<sup>48</sup> and for a CO<sub>2</sub> laser with feedback model governed by three differential equations.<sup>49</sup> From now on, we will describe laser stability using the more detailed diagrams obtained by classifying systematically the number of spikes of the laser oscillations.

Both panels on the top row of Fig. 1 contain triplets of dots labeled  $A, B, C$ ;  $D, E, F$ ; and  $G, H, I$ . Such points are the first ones of an apparently infinite sequence of analogous

points lying inside certain complex structures (shrimps<sup>13,44,47,50–52</sup>). These sequences of points accumulate towards a large region on the right-hand-side containing the number 3 and representing periodic laser oscillations with three-spikes per period. Panels (a) to (i) of Fig. 1 show how the laser signal changes along the first three of these sequences of points. The period  $T_\ell$  (arbitrary units) seems to grow continuously

$$(T_A, T_B, T_C, \dots) = (213.57, 300.32, 386.03, \dots), \quad (7)$$

$$(T_D, T_E, T_F, \dots) = (242.70, 327.61, 411.98, \dots), \quad (8)$$

$$(T_G, T_H, T_I, \dots) = (245.91, 329.97, 414.10, \dots). \quad (9)$$

But, the number of spikes shows a remarkable behavior: While the number of spikes cover uniformly the main body

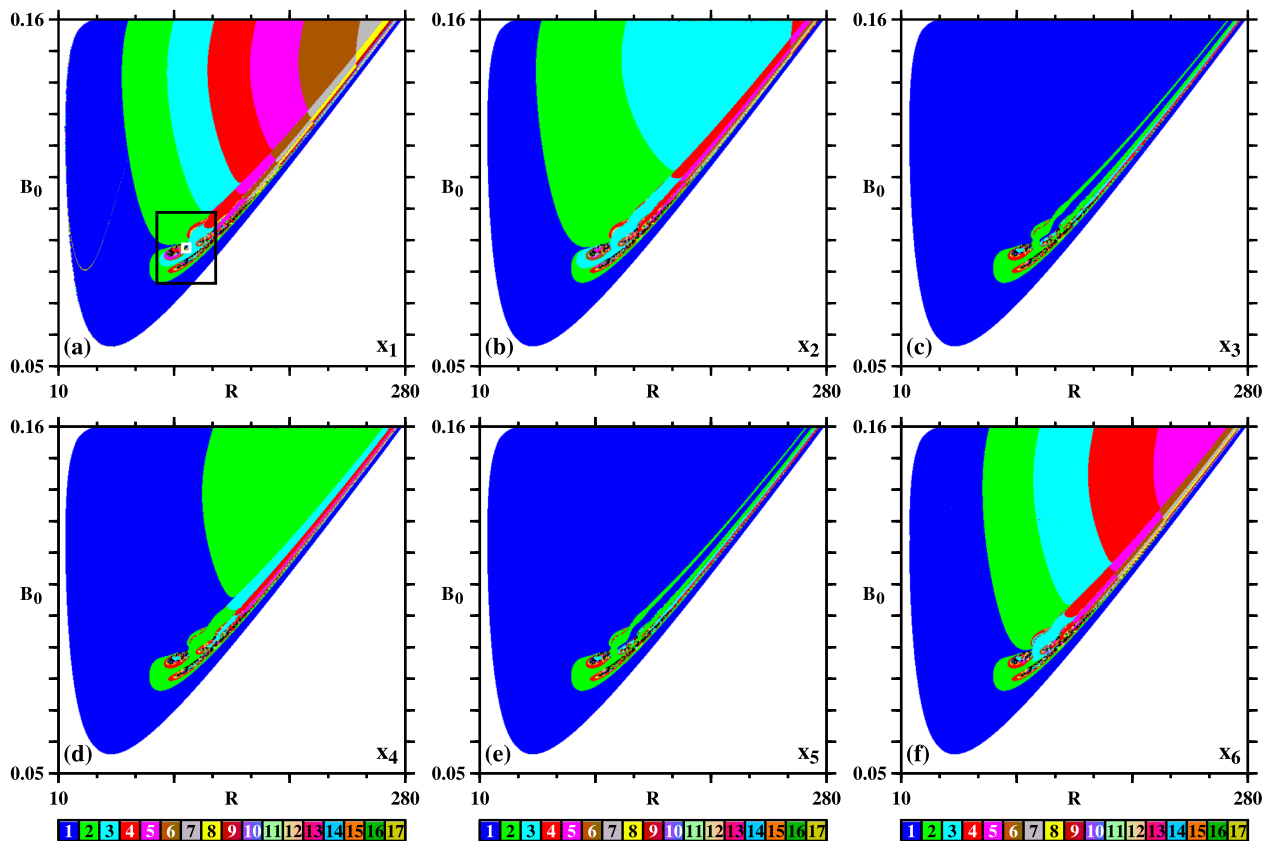


FIG. 2. Distribution of spikes as a function of the six dynamical variables used to count the spikes in one period of (a)  $x_1(t)$ , (b)  $x_2(t)$ , (c)  $x_3(t)$ , (d)  $x_4(t)$ , (e)  $x_5(t)$ , and (f)  $x_6(t)$ . Black represents chaos (i.e., non-periodic spiking). White marks a region of constant but non-zero continuous wave laser intensities. In (a), the small white rectangle at the center of the black box marks the region enlarged in Fig. 1. Chaotic laser spiking is confined to comparatively small regions.

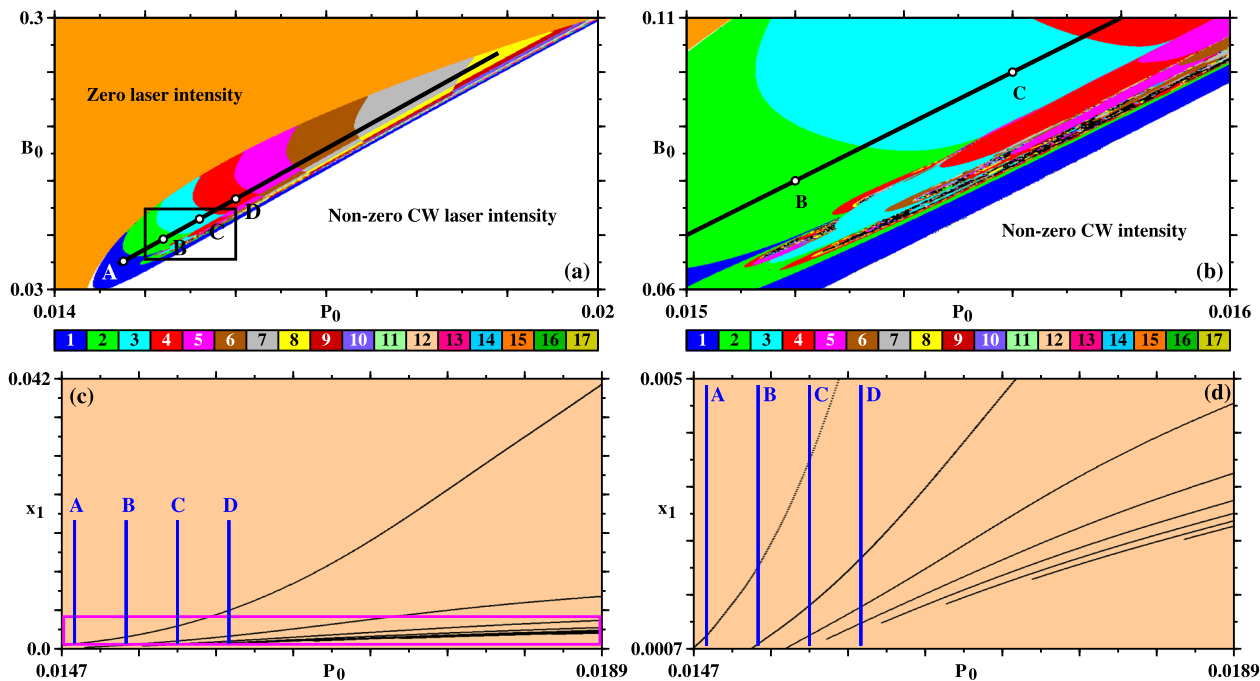


FIG. 3. (a) Nonchaos-mediated spike-adding sequences of mixed-mode oscillations<sup>45</sup> recorded in the laser intensity oscillations as a function of the pump parameter  $P_0$  and the bias voltage  $B_0$ . This control plane is dominated by large domains of zero and non-zero continuous wave laser intensities. (b) Magnification of the black rectangle seen in (a). (c) Bifurcation diagram displaying maxima of the laser intensity,  $x_1$ , illustrating the build-up of the spike-adding sequence along the black line in panels (a) and (b) when  $P_0$  and  $B_0$  are increased simultaneously. (d) Details of the spike-adding sequence inside the violet box in (c).

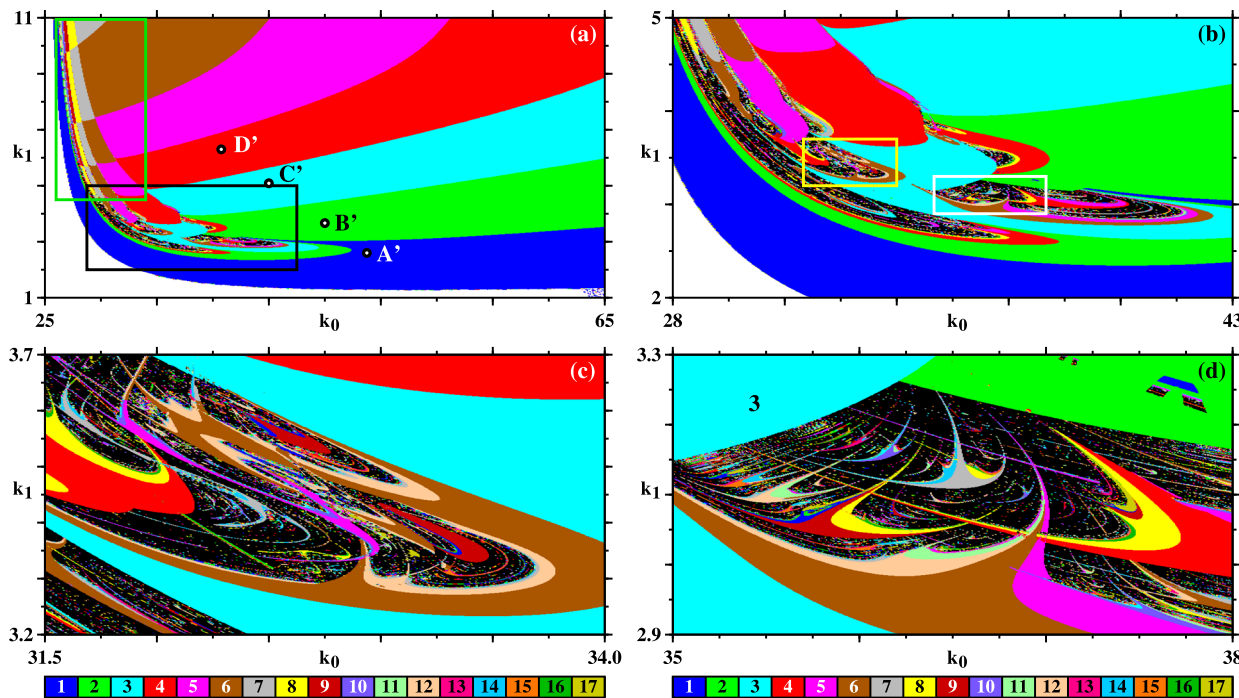


FIG. 4. (a) Nonchaos-mediated spike-adding sequences of mixed-mode oscillations recorded as a function of  $k_0$ , the control of the unperturbed cavity losses, and  $k_1$ , the modulation strength. This control plane is dominated by periodic laser spiking. The mosaic-like pattern inside the vertical rectangle is enlarged in Fig. 7. (b) Magnification of the black horizontal rectangle in (a). (c) Magnification of the leftmost rectangle in (b). (d) Magnification of the rightmost rectangle in (b). The number 3 marks the domain towards which both 3-spikes adding cascades accumulate. Note the similarity of the shrimp accumulations in this panel with the ones in Fig. 1.

of the shrimps<sup>50,51</sup> forming the sequence  $A, B, C, \dots$ , the main body of the sequences  $D, E, F, \dots$  and  $G, H, I, \dots$  are split into two separate domains characterized by distinct number of spikes. Uniform accumulations of spikes were observed before.<sup>47</sup> But, as far as we know, shrimps containing double accumulations like the sequences  $D, E, F, \dots$  and  $G, H, I, \dots$  have not been observed before. Note that all three spike-adding accumulations involve the addition of three spikes, which is the number of spikes of the domain towards which they accumulate very fast.

The time evolutions in Figs. 1(a)–1(i) suggest regularities in the steady complexification of laser patterns: Each family seems to be a concatenation of a few fixed combinations of quasi-identical patterns where the rightmost end of the wave pattern gets more and more extra spikes as one moves towards the accumulation boundary. This situation is reminiscent of behavior found recently in the Mackey-Glass delayed feedback system,<sup>48</sup> a mathematically more complicated system, described by an infinite-dimensional set of equations. A detailed investigation of these concatenated patterns will not be pursued here.

Since we consider a six dimensional model for the laser, a natural question to ask is whether or not the distribution of spikes depends on the specific dynamical variable used to count them. To check this, Fig. 2 presents six stability diagrams, one for each variable  $x_\ell$ . This figure shows unambiguously that the recorded spikes distribution depends strongly on the variable used. It is also clear that the boundaries of the spiking phases lie in different positions. Curiously, the spiking phases seem to roughly organize themselves into

three similarity classes, in the sense that each pair of variables  $(x_1, x_6)$ ,  $(x_2, x_4)$ , and  $(x_3, x_5)$  produces a somewhat similar distribution of spikes. It is also manifest that the diagrams obtained for the variables  $(x_2, x_4)$  somewhat interpolate the diagrams obtained for the pairs  $(x_1, x_6)$  and  $(x_3, x_5)$ . It is noteworthy here that while  $x_1$  (the laser output),  $x_2$  (the population inversion), and  $x_6$  (the feedback voltage) are more easy to be accessed experimentally, the remaining triplet  $x_3, x_4, x_5$ , accounting for exchanges between the molecular levels resonant with the radiation and other rotational levels within the same vibrational band, is not directly accessible to experimentation.

Figure 2 depicts a much larger region of the laser control space than the one shown in Fig. 1 and shows that the complexification of the laser intensity occurs via nonchaos-mediated mixed-mode oscillations.<sup>45</sup> Another important piece of information provided by Fig. 2 is that periodic spiking (represented by non-black phases) is by far the dominant behavior in this control plane of the laser. In other words, the black color representing chaos and seen extensively in Fig. 1, in fact, exists only in comparatively small regions of this control space. As illustrated in Figs. 3–4 and 6–8, this statement remains true for other sections of the control space.

How does the distribution of spikes looks like when recorded in other control parameter planes of the laser? This question is answered in Figs. 3–8 obtained by counting spikes of the laser intensity  $x_1$ . Figure 3 shows a global view of the control plane defined by the pump parameter  $P_0$  and the bias voltage  $B_0$ . As illustrated in Fig. 3(a), this space is dominated by large domains of zero and non-zero continuous

wave (CW) laser intensities. Separating these two domains, there is a stripe of parameters along which one sees a plethora of laser oscillations organized in a regular way. Similar to what happens in the plane  $R \times B_0$  (Fig. 2), the plane  $P_0 \times B_0$  also shows that the complexification of the laser intensity occurs via nonchaos-mediated spike-adding mixed-mode oscillations. This is corroborated clearly by the bifurcation diagrams in Figs. 3(c) and 3(d). Such diagrams were drawn by tuning both parameters,  $P_0$  and  $B_0$ , simultaneously along a portion of the black auxiliary line seen in panels (a) and (b). The vertical lines in (c) and (d) indicate the position of the four representative points  $A, B, C, D$  marked in the stability diagrams [Figs. 3(a) and 3(b)].

Figure 4 shows the distribution of laser phases recorded for the parameter section defined by the unperturbed cavity losses  $k_0$  versus the modulation strength  $k_1$ . This plane contains a remarkable feature, namely, the mosaic-like tiling that accumulates from right to left inside the vertical rectangle seen on the left side of Fig. 4(a). Such tiling consists of an apparently infinite sequence of stability phases that arises from the regular way that spikes are added to the laser intensity pulse when both parameters are tuned. As may be seen from the figure, the mosaic consists of adjacent phases characterized by waveforms where the number of spikes grows horizontally from right to left as  $k_0$  decreases, and grows from bottom to top, as  $k_1$  increases. This type of change implies the existence of two types of parameter paths—one for “horizontal” nonchaos-mediated spike-adding sequences of mixed-mode oscillations and another one, transversal, for “vertical” sequences. Note that observation of such mosaic requires tuning two parameters simultaneously, something not usually done in experiments.

The parameter region inside the rightmost rectangular box in Fig. 4(a) is shown magnified in Fig. 4(b), and the pair of boxes in it are enlarged in Figs. 4(c) and 4(d). Figures 4(c) and 4(d) illustrate regions where chaos is quite abundant. Figure 4(c) shows a typical configuration found in many places in control space: oscillatory laser modes emerge organized in very complicated ways which are simply too complex to be described by other than graphical means. In sharp contrast, Fig. 4(d) shows infinite sequences of phases displaying the same regular spike-adding systematics already found in the upper panels in Fig. 1, accumulating also

towards a large laser phase where the intensity pulses contain three spikes per period.

How similar are the mixed-mode oscillations observed in the CO<sub>2</sub> laser with feedback when parameters are tuned? The answer is given in Fig. 5, which illustrates the great similarity of mixed-mode oscillations typically observed when tuning rather distinct control parameters of the laser. In the top row of Fig. 5, we plot the first four of an apparently infinite sequence of consecutive spike additions observed in the  $P_0 \times B_0$  control plane. These four panels correspond to the points labeled  $A, B, C, D$  in Fig. 3(a), with coordinates  $(P_0, B_0) = (0.0148, 0.06), (0.0152, 0.08), (0.0156, 0.1), (0.016, 0.12)$ , respectively. For comparison, the bottom row shows an analogous sequence, but observed while tuning parameters in the  $k_0 \times k_1$  plane for points  $A', B', C', D'$  in Fig. 4(a), with coordinates  $(k_0, k_1) = (48, 2.6), (45, 3.666), (41, 5.088), (37.3, 6.404)$ , respectively. Noteworthy is the fact that, although the periods of both sequences of spikes are initially very different, after just four spike additions, they already are of the same order of magnitude, suggesting that the growth of the period may not be unbounded.

Figure 6(a) shows a global description of the spike unfolding recorded on the  $R \times P_0$  control plane. This plane also shows regular laser pulsations organized according similar spike-adding scenarios as previously found in other control planes. In contrast with previous situations, in this parameter plane it is quite easy to follow spike-adding sequences by tuning just a single parameter,  $R$ , instead of a pair of parameters, as before. Furthermore, as illustrated in Figs. 6(b) and 6(c), it is not any path across the control space that will reveal its regular organization and mixed-mode oscillations. For instance, as depicted in panels 6(d)–6(f), bifurcations along vertical one-parameter lines will typically result in rather unusual series of spikes, mediated or not by chaos. To uncover the mechanism responsible for such complex and apparently non-systematic spike unfoldings remains an open challenge.

The temporal evolutions in Figs. 6(d)–6(f) show a close resemblance to those in Fig. 5, despite the fact that they are obtained by sweeping rather distinct parameters. The high number of parameters involved and the great variety of spikes arrangements that were observed prevents one from attempting a general classification. But, such classification is

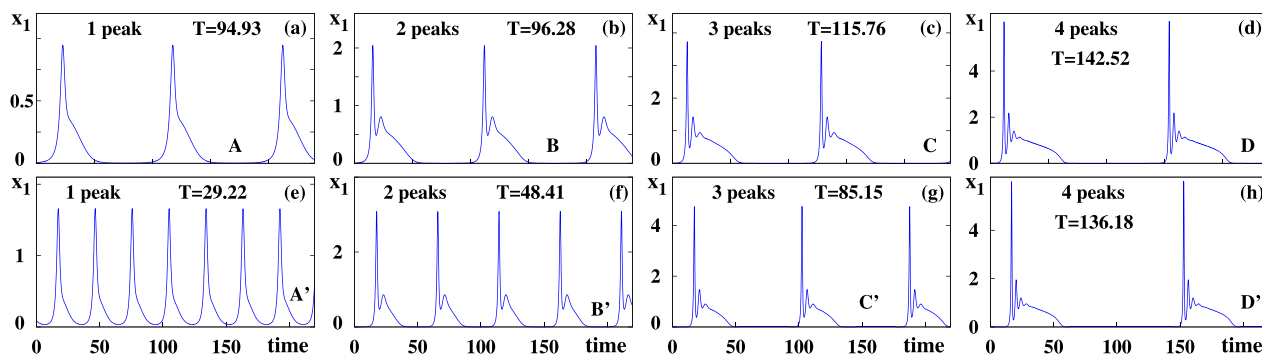


FIG. 5. Two similar looking sequences of spike-adding mixed-mode oscillations recorded while tuning rather distinct laser control parameters. Top row: temporal evolutions for points labeled  $A, B, C, D$  on the  $P_0 \times B_0$  plane of Fig. 3(a). Bottom row: temporal evolutions for points  $A', B', C', D'$  on the  $k_0 \times k_1$  plane of Fig. 4(a). Here,  $T$  indicates the period of the oscillations in arbitrary units. For convenience, the vertical axis shows  $10^3 x_1$ .

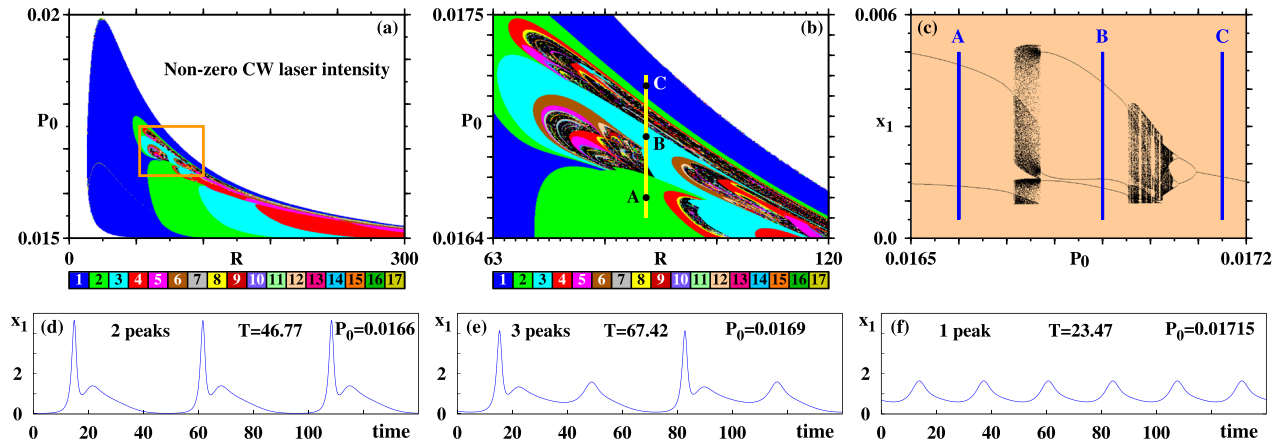


FIG. 6. (a) Global view of the spikes distribution in the  $R \times P_0$  plane illustrating spike-adding cascades and predominance of CW laser modes. (b) Magnification of the box in (a) showing (in black) the presence of chaotic laser bursting. (c) Bifurcation diagram displaying intensity maxima obtained for  $R = 89$ , along the vertical line in (b). (d)–(f) Laser intensity for A, B, C as indicated in panels (b) and (c). Here,  $T$  denotes the period of the oscillation (arbitrary units). For convenience, the vertical axis shows  $10^3 x_1$ .

obviously an important and enticing problem that needs to be eventually addressed.

We now investigate what happens with the laser intensity in Fig. 7(a), a magnification of the leftmost (vertical) rectangle in Fig. 4(a). As already mentioned, this region contains large stability phases forming a mosaic-like tiling that accumulates in Fig. 7(a) from right to left and from bottom to top. We consider the waveforms along two representative stripes of such tiling: for the points A, B, C along the line  $k_1 = 8.5$ , and for points D, E, F along  $k_1 = 6.5$ . As evidenced by Figs. 7(b)–7(g), the complexification of the waveforms underlying the mosaic-like tiling involve two concurrent mechanisms which act on the large plateau contained in the periodic oscillations: when parameters are tuned, the plateau develops more and more undulations on both extremities. On the left-hand-side of the plateau, one finds a complexification that unfolds in a similar way as already described in Fig. 5 for the mixed-mode oscillations. The novelty here is that, simultaneously, there is a

complexification at the right-hand-side extremity of the plateau, also by the addition of spikes. Thus, the mosaic-like tiling accumulation seems to originate from a double winding of the trajectories in phase-space. While double windings have certainly been described abundantly in connection with homoclinic orbits and with other sophisticated forms of unstable mathematical phenomena, we are not aware of the impact of any of these phenomena being described in parameter space. In contrast with unstable homoclinic phenomena, the double winding mentioned here (i) is manifestly connected with stable trajectories, (ii) is clearly responsible for inducing regularities in large portions of the control parameter space. Recall that, while there is a profusion of studies dealing with the intricacies of complex phenomena in phase-space, most of them refer to systems whose laboratory implementation is difficult. Our diagrams, however, display the global organization of stability phases and, therefore, are directly measurable with present day technology. For instance, a recent comparison between measurements and

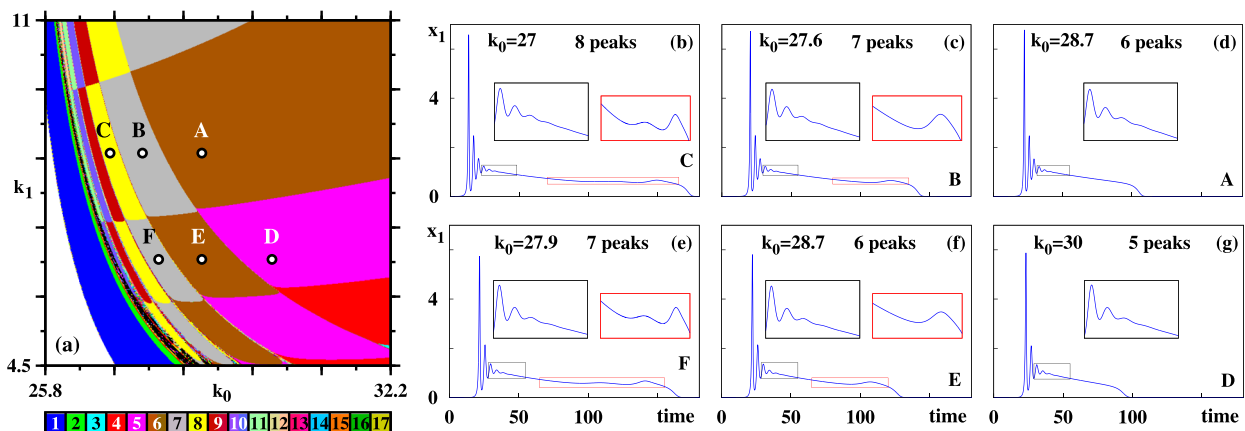


FIG. 7. (a) Enlargement of the vertical rectangle in Fig. 4(a) illustrating the a mosaic-like pattern and remarkable systematic shifts of the laser pulsations. (b)–(g) Temporal evolutions of the laser pulses showing the genesis of new spikes [through waveform deformations<sup>48,49</sup>] underlying the mosaic-like pattern. The respective period of oscillation are  $T_A = 300.58$ ,  $T_B = 342.09$ ,  $T_C = 377.97$ ,  $T_D = 172.47$ ,  $T_E = 210.46$ , and  $T_F = 245.92$ , in arbitrary units. Such tiling repeats over an extended region of the control space. For convenience, the vertical axis shows  $10^3 x_1$ .

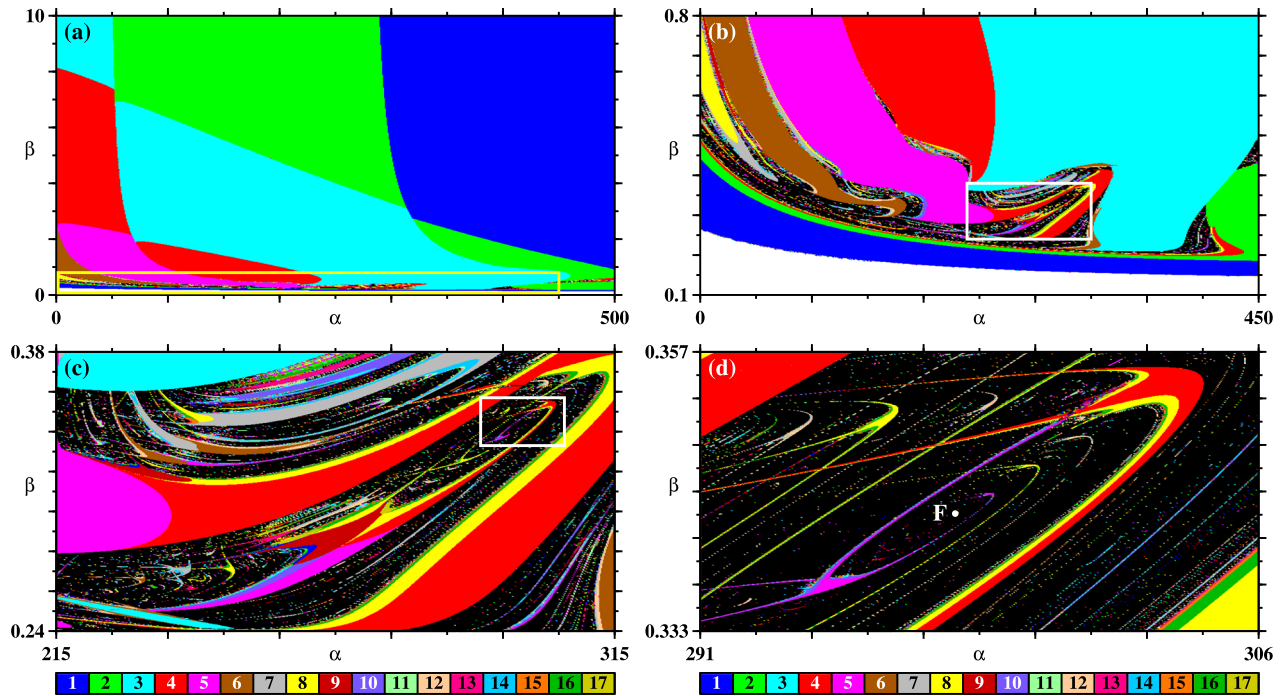


FIG. 8. (a) Mosaic-like pattern in the bandwidth  $\alpha$  versus amplification  $\beta$  control plane. (b) Magnification of the box in (a) illustrating the presence of “wrinkles” (see text). (c) Magnification of the box in (b). (d) Magnification of the box in (c) illustrating an infinite hierarchy of nested spirals of chaos and of regularity converging to the focal hub  $F$  near  $(\alpha, \beta) = (297.85, 0.3431)$ .

predictions for an electronic device found them to be in rather good agreement over wide two-dimensional control parameter windows.<sup>43</sup>

Is the mosaic-like tiling a particularity of the  $k_0 \times k_1$  control plane (Fig. 7), or is it a generic feature? To check this, we computed high-resolution phase diagrams for the control plane defined by the bandwidth  $\alpha$  and amplification  $\beta$  of the laser, shown in Fig. 8. As it is evident from Fig. 8(a), this control plane also displays a mosaic-like tiling. As before, this plane shows a large predominance of periodic over chaotic laser modes.

At the bottom of Fig. 8(a) one sees a thin rectangular box, shown magnified in Fig. 8(b). From this magnification, one sees that chaos (represented in black) arises from certain “wrinkles” that develop in the phases of regularity that, for larger values of  $\beta$ , combine to form the mosaic-like tiling. Although chaotic phases are quite small compared to the overwhelmingly large regular phases, they can be probed experimentally without problem with modern technology. In fact, as discussed in Sec. II, chaos in CO<sub>2</sub> lasers with feedback was already reported in many experiments. What is still open is a systematic experimental scan of the control parameter space, similar to what was done here numerically. Experimental scans can either corroborate the modeling or uncover shortcomings of the equations used in the numerical analysis.

The chaotic phases of the CO<sub>2</sub> laser with feedback are full of rich dynamics, also waiting for a systematic exploration. For instance, Fig. 8(c) shows a magnification of the box in Fig. 8(b). This figure illustrates once again the complex alternation of chaotic and regular stability phases of the lasers, similar to the situation described above for Fig. 4(c).

However, chaotic phases also harbor wide regions of regularity, as exemplified by Fig. 8(d), an enlargement of the rectangle in Fig. 8(c). Figure 8(d) illustrates an infinite sequence of spirals of chaos and spirals of regularity that arise around certain exceptional points in control space, called periodicity hubs, well-known to organize the dynamics over extended parameter regions.<sup>44,53–57</sup> The exceptional point responsible for the large anti-clockwise spiraling in Fig. 8(d) is located at the periodicity hub  $F$ , numerically estimated to be near  $F = (\alpha, \beta) = (297.85, 0.3431)$ . An infinite quantity of similar hubs is known to exist in the vicinity of  $F$ , as elaborated in Refs. 55 and 56. Summarizing, intricate alternations of chaos and regularity can be observed abundantly in every section of the control space.

## VI. CONCLUSIONS

We presented an exhaustive analysis of the control parameter space of the CO<sub>2</sub> laser in the sense that all major combinations of control parameters were considered. This is a significant addition to the field and opens new possibilities of investigation. Earlier experiments considered only the bias  $B_0$  as variable, keeping all other parameters fixed. After that, the influence of the bandwidth  $\beta$  was also considered. Experimentally, it is clear that  $k_0$  and  $k_1$  are difficult to tune although something could be done. Changes of the pump parameter  $P_0$  were not yet considered. However, as shown by Figs. 3, 5, and 6, variations of  $P_0$  produce quite interesting results. The parameters  $\beta$  and  $\alpha$  are difficult to scan experimentally, in particular,  $\alpha$  which is related to the saturation in the detection of the laser intensity. Thus, the stability diagrams reported here suggest a number of new and interesting

experimental explorations. Furthermore, they predict explicitly parameter intervals likely to contain rich dynamics.

From the point of view of simulations, the stability diagrams for the six dimensional model corroborate previous findings obtained for the simpler three dimensional model,<sup>49</sup> but go well beyond them. Considering the relevance of the CO<sub>2</sub> laser with optoelectronic feedback in nonlinear dynamics, a detailed investigation taking advantage from the novel isospike technique<sup>39–46</sup> has been proposed. In isospike diagrams, new dynamical features related to the organization of stable spiking and bursting behavior emerge for accessible parameter values. A significant observation is that qualitatively similar organizations of laser spiking and bursting can be obtained by tuning rather distinct control parameters. In other words, not only the stability phases look similar when recorded in distinct control planes, but the spikes unfold in a similar way over extended parameter intervals. This fact strongly suggests the existence of unexpected symmetries in the laser control space. It is important to stress that, in any phase diagram, systematic trends become clear only when recording the dynamics on a fine mesh and while varying at least two independent parameters simultaneously, a procedure that is not yet common in experimental work.

Although the six dimensional model for the CO<sub>2</sub> laser with opto-electronic feedback has been introduced and accurately tested for this kind of molecular laser, it could be considered in different applications spanning from secure communications to modelling brain dynamics, when the intrinsic time-scales associated with fast and slow variables are carefully adjusted and tailored to a specific problem, that is, the millisecond range. In fact, in several diagrams, we observe that the number of spikes in one period increases following a recently reported nonchaos mediated spike adding mechanism. In such case, we can approach the time scales typical of neuronal brain phenomena, making the dynamical features observed here to be also attractive for analogies in neuroscience.

While the spike unfolding occurring over wide parameter regions where periodic oscillations dominate seems to be fairly well understood, the classification of the very complex combinations of chaotic and non-chaotic phases demand much more investment of computer time and experimentation. The big open challenge is to classify wave pattern complexification by peak-deformations when several parameters are tuned simultaneously.

## ACKNOWLEDGMENTS

J.G.F. was supported by Post-Doctoral Grant No. SFRH/BPD/43608/2008 from FCT, Portugal. R.M. and F.T.A. acknowledge financial support from *Fondazione Ente Cassa di Risparmio di Firenze*. All bitmaps were computed at the CESUP-UFRGS clusters, Porto Alegre, Brazil. This work was supported by the Deutsche Forschungsgemeinschaft through the Cluster of Excellence *Engineering of Advanced Materials* and by the Max-Planck Institute for the Physics of Complex Systems, Dresden, in the framework of the Advanced Study Group on Optical Rare Events.

- <sup>1</sup>C. K. N. Patel, *Phys. Rev.* **136**, A1187 (1964).
- <sup>2</sup>W. Zinth, A. Laubereau, and W. Kaiser, *Eur. Phys. J. H* **36**, 153 (2011).
- <sup>3</sup>E. J. Doedel and C. L. Pando L., *Phys. Rev. E* **89**, 052904 (2014).
- <sup>4</sup>E. J. Doedel, B. Krauskopf, and C. L. Pando L., *Eur. Phys. J. Spec. Top.* **223**, 2847 (2014).
- <sup>5</sup>A. Uchida, F. Rogister, J. Garcia-Ojalvo, and R. Roy, *Progress in Optics*, edited by E. Wolf (Elsevier, Dordrech, 2005), Vol. 48.
- <sup>6</sup>*Digital Communications Using Chaos and Nonlinear Dynamics*, edited by L. E. Larson, J. M. Liu, and L. S. Tsimring (Springer, NY, 2006).
- <sup>7</sup>I. Susa, T. Erneux, A. Barsella, C. Lepers, D. Dangoisse, and P. Glorieux, *Phys. Rev. A* **63**, 013815 (2000).
- <sup>8</sup>F. T. Arecchi, R. Meucci, G. Puccioni, and J. Tredicce, *Phys. Rev. Lett.* **49**, 1217 (1982).
- <sup>9</sup>V. Zehnlé, D. Dangoisse, and P. Glorieux, *Opt. Commun.* **90**, 99 (1992).
- <sup>10</sup>D. Dangoisse, P. Glorieux, and D. Hennequin, *Phys. Rev. Lett.* **57**, 2657 (1986).
- <sup>11</sup>D. Dangoisse, P. Glorieux, and D. Hennequin, *Phys. Rev. A* **36**, 4775 (1987).
- <sup>12</sup>M. Lefranc and P. Glorieux, *Int. J. Bifur. Chaos* **3**, 643 (1993).
- <sup>13</sup>C. Bonatto, J. C. Garreau, and J. A. C. Gallas, *Phys. Rev. Lett.* **95**, 143905 (2005).
- <sup>14</sup>F. T. Arecchi, W. Gadomski, and R. Meucci, *Phys. Rev. A* **34**, 1617 (1986).
- <sup>15</sup>F. T. Arecchi, G. L. Lippi, G. P. Puccioni, and J. R. Tredicce, *Optics Commun.* **51**, 308 (1984).
- <sup>16</sup>F. T. Arecchi, R. Meucci, and W. Gadomski, *Phys. Rev. Lett.* **58**, 2205 (1987).
- <sup>17</sup>J. Duprè, F. Meyer, and C. Meyer, *Rev. Phys. Appl. (Paris)* **10**, 285 (1975).
- <sup>18</sup>E. Arimondo, F. Casagrande, L. A. Lugiato, and P. Glorieux, *Appl. Phys. B* **30**, 57 (1983).
- <sup>19</sup>M. L. Asquini and F. Casagrande, *Nuovo Cimento D* **2**, 917 (1983).
- <sup>20</sup>M. Tachikawa, F. L. Hong, K. Tanii, and T. Shimizu, *Phys. Rev. Lett.* **60**, 2266 (1988).
- <sup>21</sup>D. Dangoisse, A. Bekkali, F. Papoff, and P. Glorieux, *Europhys. Lett.* **6**, 335 (1988).
- <sup>22</sup>A. R. Zeni, J. A. C. Gallas, A. Fioretti, F. Papoff, B. Zambon, and E. Arimondo, *Phys. Lett. A* **172**, 247 (1993).
- <sup>23</sup>Y. Liu, P. C. de Oliveira, M. B. Danailov, and J. R. Rios Leite, *Phys. Rev. A* **50**, 3464 (1994).
- <sup>24</sup>P. Alcantara, Jr., L. Guidoni, A. Barsella, A. Fioretti, and E. Arimondo, *J. Opt. Soc. Am. B* **12**, 1326 (1995).
- <sup>25</sup>*Laser Dynamics*, edited by T. Erneux and P. Glorieux (Cambridge University Press, Cambridge, 2010).
- <sup>26</sup>F. T. Arecchi, W. Gadomski, R. Meucci, and J. A. Roversi, *Opt. Commun.* **65**, 47 (1988).
- <sup>27</sup>P. Mandel and T. Erneux, *Phys. Rev. Lett.* **53**, 1818 (1984).
- <sup>28</sup>F. T. Arecchi, W. Gadomski, R. Meucci, and J. A. Roversi, *Opt. Commun.* **70**, 155 (1989).
- <sup>29</sup>R. Meucci, M. Ciofini, and P. Y. Wang, *Opt. Commun.* **91**, 444 (1992).
- <sup>30</sup>A. Varone, A. Politi, and M. Ciofini, *Phys. Rev. A* **52**, 3176 (1995).
- <sup>31</sup>R. Meucci, A. Labate, and M. Ciofini, *Phys. Rev. E* **56**, 2829 (1997).
- <sup>32</sup>M. Ciofini, A. Labate, R. Meucci, and M. Galanti, *Phys. Rev. E* **60**, 398 (1999).
- <sup>33</sup>E. Allaria, F. T. Arecchi, A. Di Garbo, and R. Meucci, *Phys. Rev. Lett.* **86**, 791 (2001).
- <sup>34</sup>F. T. Arecchi, E. Allaria, and I. Leyva, *Phys. Rev. Lett.* **91**, 0234101 (2003).
- <sup>35</sup>I. Leyva, E. Allaria, F. T. Arecchi, and S. Boccaletti, *Phys. Rev. E* **68**, 066209 (2003).
- <sup>36</sup>A. N. Pisarchik, R. Meucci, and F. T. Arecchi, *Eur. Phys. J. D* **13**, 385 (2001); *Phys. Rev. E* **62**, 8823 (2000).
- <sup>37</sup>*Nonlinear Dynamics and Chaos with Applications to Physics, Biology, Chemistry, and Engineering*, 2nd ed., edited by S. Strogatz (Westview Press, Boulder, 2015).
- <sup>38</sup>*An Exploration of Dynamical Systems and Chaos*, edited by J. Argyris, G. Faust, M. Haase, and R. Friedrich (Springer, New York, 2015).
- <sup>39</sup>J. G. Freire and J. A. C. Gallas, *Phys. Chem. Chem. Phys.* **13**, 12191 (2011).
- <sup>40</sup>J. G. Freire and J. A. C. Gallas, *Phys. Lett. A* **375**, 1097 (2011).
- <sup>41</sup>J. G. Freire, T. Pöschel, and J. A. C. Gallas, *Europhys. Lett.* **100**, 48002 (2012).
- <sup>42</sup>S. L. T. Souza, A. A. Lima, I. R. Caldas, R. O. Medrano-T, and Z. O. Guimarães-Filho, *Phys. Lett. A* **376**, 1290 (2012).

- <sup>43</sup>A. Sack, J. G. Freire, E. Lindberg, T. Pöschel, and J. A. C. Gallas, *Sci. Rep.* **3**, 3350 (2013).
- <sup>44</sup>M. R. Gallas, M. R. Gallas, and J. A. C. Gallas, *Eur. Phys. J. Spec. Top.* **223**, 2131 (2014).
- <sup>45</sup>M. J. B. Hauser and J. A. C. Gallas, *J. Phys. Chem. Lett.* **5**, 4187 (2014).
- <sup>46</sup>A. Hoff, D. T. da Silva, C. Manchein, and H. A. Albuquerque, *Phys. Lett. A* **378**, 171 (2014).
- <sup>47</sup>C. Bonatto and J. A. C. Gallas, *Phil. Trans. R. Soc. A* **366**, 505 (2008).
- <sup>48</sup>L. Junges and J. A. C. Gallas, *Phys. Lett. A* **376**, 2109 (2012).
- <sup>49</sup>L. Junges and J. A. C. Gallas, *Opt. Comm.* **285**, 4500 (2012).
- <sup>50</sup>J. A. C. Gallas, *Phys. Rev. Lett.* **70**, 2714 (1993).
- <sup>51</sup>J. A. C. Gallas, *Physica A* **202**, 196 (1994).
- <sup>52</sup>E. N. Lorenz, *Physica D* **237**, 1689 (2008).
- <sup>53</sup>C. Bonatto and J. A. C. Gallas, *Phys. Rev. Lett.* **101**, 054101 (2008).
- <sup>54</sup>J. G. Freire and J. A. C. Gallas, *Phys. Rev. E* **82**, 037202 (2010).
- <sup>55</sup>J. A. C. Gallas, *Int. J. Bifurc. Chaos* **20**, 197 (2010).
- <sup>56</sup>R. Vitolo, P. Glendinning, and J. A. C. Gallas, *Phys. Rev. E* **84**, 016216 (2011).
- <sup>57</sup>R. Barrio, F. Blesa, S. Serrano, and A. Shilnikov, *Phys. Rev. E* **84**, 035201 (2011).